Electron bolus design for radiotherapy treatment planning: Bolus design algorithms

D. A. Low,[a] G. Starkschall, S. W. Bujnowski, L. L. Wang, and K. R. Hogstrom
Department of Radiation Physics, The University of Texas M. D. Anderson Cancer Center, 1515 Holcombe Boulevard, Houston, Texas 77030

(Received 2 January 1991; accepted for publication 23 April 1991)

Computer algorithms to design bolus for electron beam radiotherapy treatment planning were investigated. Because of the significant electron multiple scatter, there is no unique solution to the problem of bolus design. However, using a sequence of operators, a bolus can be designed that attempts to meet three important criteria: adequate dose delivery to the target volume, avoidance of critical structures, and dose homogeneity within the target volume. Initial calculation of bolus shape was based upon creation operators forcing either the physical or the effective depths of the distal surface of the target volume to a specified value. Modification operators were then applied to the bolus to alter the shape to better meet the design criteria. Because the operators each address a single dosimetric issue, they can often adversely affect some other attribute of the dose distribution. In addition, an extension operator is used to design the bolus thickness outside the target volume. Application of these operators is therefore carried out in certain sequences and each may be used more than once in the design of a particular bolus. The effects of these operators on both the bolus and the resulting dose distribution are investigated for test geometries and patient geometries in the nose, parotid, and paraspinal region.

Key words: electron beam radiotherapy, electron bolus design, electron conformal therapy

I. INTRODUCTION

Electron beams of energy 20 MeV or less are useful in treating tumors to depths of usually 6 cm or less. In a water phantom an electron beam provides a relatively uniform dose ($\pm$ 10%) to a volume just inside the perceived treatment volume defined by the field collimation and the depth of the 90% depth dose, R_{90}. The finite range of electrons in tissue results in a sharp falloff of dose at depths beyond R_{90}, protecting critical structures and normal tissues. However, in an actual patient, tumor underdose, critical structure overdose, or nonuniform dose in the target volume can occur. These can be caused either by skin surface or internal heterogeneities, as discussed by Hogstrom[1] and Hogstrom and Fields,[2] or by a highly variable depth of the distal surface of the target volume. To reduce such effects, electron bolus is used in an effort to conform the therapeutic, 90% isodose contour to the target volume while maintaining a reasonably uniform dose inside.

Electron bolus in radiotherapy has three applications. The first is to increase the dose to the patient's external surface.[3-5] The second is to serve as a missing tissue compensator, accounting for surface irregularities and internal heterogeneities.[6] The third is to shape the coverage of the treatment volume to conform as closely as possible to the target volume and to avoid critical structures by accounting for the variable depth of the distal surface of the target volume.[7-9] This work focuses on the latter two applications, using bolus to either eliminate or decrease the adverse effects of patient heterogeneities on the dose distribution, which can result in a geographical miss in depth, dose nonuniformity within the target volume, and excessive dose to critical structures.

Implementation of a general-use clinical program for electron bolus requires three components: design, fabrication, and verification. The emphasis of the present work will be on bolus design and prefabrication verification. Prefabrication verification requires the ability to accurately calculate the patient dose in three dimensions (3D) while incorporating the presence of bolus. This is done in the present work using a 3-D implementation of the pencil-beam algorithm.[10] Bolus has been fabricated using a computer-controlled milling machine similar to that used by Smith *et al.*[11]

Several sophisticated methods for clinical bolus programs have been used for pions,[12-14] protons,[15-19] and heavy ions.[20] Bolus design in these cases was simpler in that multiple Coulomb scatter (MCS) is small enough so that bolus could be designed based solely on requiring constant radiological depth from the bolus surface to the distal surface of the volume. On the other hand, lack of significant MCS led to concerns regarding small patient movement or bolus misalignment.[19,21]

For electrons, previous investigators[11,22,23] have designed bolus such that the depth (along a fan line) from the bolus surface to the distal edge of the target volume is constant and equals the central-axis depth of the therapeutic isodose contour (e.g., R_{80} or R_{90}). In some cases the therapeutic depth was allowed to vary with off-axis position. These methods suffered from a variety of limitations. First, a 2-D approximation was used, assuming the radiation source to lie in the plane in which bolus was designed.[11] In the present work, this is resolved by treating the problem in its true 3-D sense. Second, the extension of bolus to areas outside the projection of the target volume was inadequately developed. Methods and options for bolus extension are therefore also presented. Third, most bolus design methods for electrons have ignored

 0094-2405/92/010115-10$01.20

differences in tissue densities by assuming the patient is of unit density. The effects of internal air cavities (e.g., sinuses), however, can be significant in the head, neck, and lungs. Heavy particle bolus designs, because of these particle's much deeper penetration, have accounted for tissue inhomogeneities by designing bolus for a constant radiological rather than physical depth.

The most significant deficiency in prior approaches to design of electron bolus is that these approaches typically have been one-dimensional in nature, assuming that electrons travel in straight lines and are not scattered. The effect of multiple Coulomb scattering is illustrated in Fig. 1(a). Note that the radial fluence distribution for a pencil beam at depth is Gaussian in shape, so that the bolus thickness along a fan line influences dose throughout the neighboring region. Figure 1(b) illustrates the paths of three sets of electrons. Each set begins in the same pencil beam, but traverses through different amounts of air heterogeneity to reach points A, B, and C at the distal surface of the target volume. The effective depths of the distal surface of the target volume is thus different along each electron path, hence the amount of bolus required to be placed in the path of the pencil beam to make the distal surface of the target volume at a uniform depth will be different. There are three different solutions, supporting a very important hypothesis: there is no unique solution to the bolus design problem. In Fig. 1(c), a bolus design ignoring the effects of multiple Coulomb scatter is shown to have two difficulties: (1) the sharp edge of the bolus results in a "hot/cold spot"[24], and (2) the therapeutic isodose (90%) does not track the target volume. This problem was acknowledged by Smith *et al.*,[11] who indicated that bolus shape can be modified after subsequent dose calculations. This work expands those concepts by developing tools for such a process, i.e., fully 3-D dose calculations and bolus operators.

The problem of bolus design has been approached recognizing that there is, in fact, no perfect solution. A set of bolus design operators, which are tools that can be used to design an acceptable bolus, has been created. The use of these operators is illustrated for selected phantom and patient geometries. No attempt to design an optimal bolus shape is attempted since this requires a method of evaluating the utility of a bolus by comparing the resulting dose distribution to the specified dose distribution. However, in the future, these bolus design operators could prove useful in generating optimizing methods.

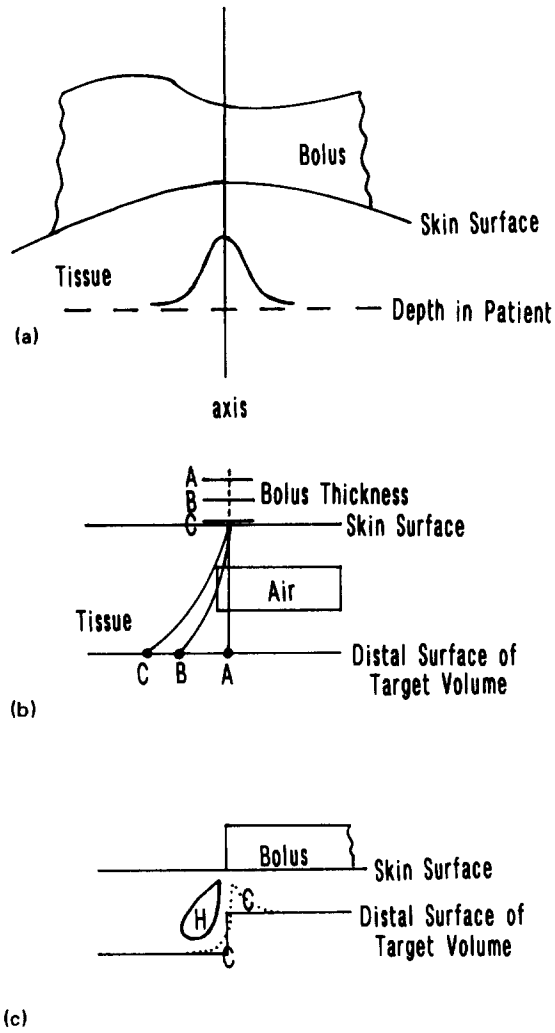

FIG. 1. Schematic representation of the influence of electron scatter on bolus design. (a) For a pencil beam of electrons incident on the bolus along the indicated central axis fan line, the dose distribution at depth in the patient is approximately Gaussian. (b) For electrons incident on a bolus along the fan line aiming toward point A, the desired bolus thickness for electrons reaching points A, B, or C is different, depending upon the amount of air intersected by the indicated mean paths. (c) A bolus that is designed ignoring multiple Coulomb scattering simply reflects the shape of the distal surface of the target volume. This bolus results in areas of increased dose (hot spot *H*) and areas of decreased dose (cold spot *C*) due to electron scatter. The therapeutic isodose (90%) is shown with a dotted line.

II. METHODS

A. Bolus design

Electron bolus is specified by its thickness along each fan line from the skin surface back toward the virtual source[25] by the variable $b = b(x,y)$, where x and y are the lateral coordinates in the (diverging) fan-line coordinate system of the beam. In practice, bolus thickness is determined on a rectangular grid as illustrated in Fig. 2(a). The grid spacing Δx, Δy is usually specified at isocenter and is the same as the dose calculation grid,[10] which is typically 2.5 mm. The grid extends outside the collimator sufficiently to encompass the beam's penumbra. This is currently done using a rectangle parallel to the x and y axes.

The bolus calculation geometry is further defined in Fig. 2(b), where terms in a plane containing central axis and the (i,j) fan line are defined. The bolus thickness, $b_{ij} = b(x_i,y_j)$, is the distance $(r_4 - r_2)_{ij}$ between points 2 and 4, where r_k is the distance between the source and point k. The physical depth of the distal surface of the target volume from the surface d_{ij} is the distance $(r_5 - r_4)_{ij}$. The physical depth of the proximal surface of a critical structure from the surface c_{ij} is the distance $(r_6 - r_4)_{ij}$. The position of the skin surface from the SSD plane s_{ij} is the distance $(r_4 - r_3)_{ij}$.

As previously discussed, there is, to our knowledge, no

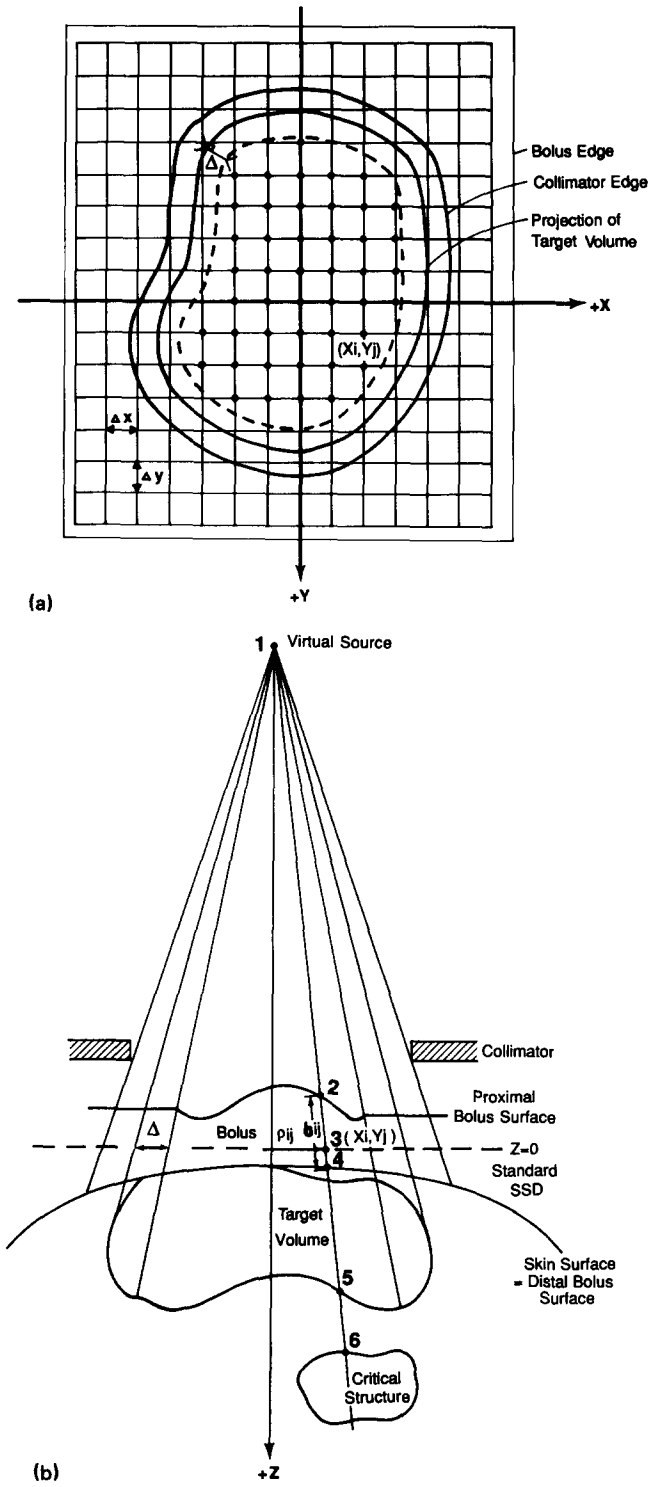

FIG. 2. (a) Schematic representation of the bolus design fan grid intersecting a plane perpendicular to the central axis at the isocenter. The outer solid curved line indicates the fan-projection of the collimator (or "cut-out") edge while the inner solid line indicates the projection of the lateral extent of the target volume. The dashed line represents the applied bolus "margin," a distance Δ inside the lateral extent of the target volume. The bolus definition points (fan lines) within the dashed contour are indicated by dots. The bolus creation operators are allowed to operate on only these points. (b) Sketch illustrating the fan geometry and design elements of the bolus design system. The design elements are illustrated through the representation of one fan line on which points 1 through 6 are drawn. Point 1 represents the virtual electron source. Points 2 through 6 represent the intersections of the fan line with the proximal bolus surface, the standard SSD plane (shown by a dashed line), the proximal patient surface, the distal target volume surface, and the proximal critical structure surface, respectively.

unique solution to the bolus design problem. Therefore, we have defined operators that are used to design a bolus that provides a clinically acceptable dose distribution. These operators transform one set of bolus thicknesses $\{b_{ij}\}$ into another. There are three classes of operators—creation, modification, and extension operators.

B. Creation operators

Creation operators provide the initial estimate of the bolus thicknesses. The first of these operators **P** designs bolus so that the distance along fan lines from the proximal surface of the bolus to the distal surface of the target volume be constant for a water-equivalent bolus. Correcting for the non-water equivalence of the bolus,

$$b_{ij} = (1/\rho_b)(R_t - d_{ij}), \tag{1}$$

where R_t is the desired therapeutic range and ρ_b is the effective density[26] of the bolus material. Typically, R_t will be specified in the range of the 80% to 90% depth dose, R_{80} to R_{90}, respectively. This type of bolus design has been reported by Beach *et al.*[8] and Smith *et al.*[11] This type of design can be improved if the variation in therapeutic depth with off-axis position is incorporated, i.e.,

$$b_{ij} = (1/\rho_b)[(R_t)_{ij} - d_{ij}]. \tag{2}$$

Archambeau *et al.*[7] used this technique in designing bolus to place the 80% isodose surface on the lung–chest wall interface.

Because the cross section of a target volume is generally rounded near its lateral boundary (cf. Fig. 2), the d_{ij} near the boundaries is usually significantly smaller than that over the neighboring internal regions of the target volume. Large bolus thicknesses calculated by Eq. (1) near these boundaries give rise to large amounts of electron scatter into the center of the radiation field, yielding unacceptably high dose values. Designing the bolus only over the interior of the target volume minimizes this problem. Therefore, bolus thickness is designed only along those rays that lie at least a distance of Δ inside the target volume (cf. Fig. 2). This region is referred to as "target volume less margin (TVLM)." The bolus margin Δ ranges typically from 0.5 to 1.5 cm. Hence, the operator **P** depends on two parameters, Δ and R_t, so $\mathbf{P} = \mathbf{P}(\Delta, R_t)$.

The initial bolus thickness can also be determined using the effective depth[26] of the distal surface of the target volume, also referred to as the water-equivalent or radiological depth. This operator **R** designs the bolus such that water-equivalent distance along fan lines from the proximal surface of the bolus to the distal surface of the target volume will be constant:

$$b_{ij} = \frac{1}{\rho_b}\left(R_t - \int_{r_4}^{r_5} \rho(r')dr'\right), \tag{3}$$

where $\rho(r')$ is the effective density of tissue[26] at location r' along the fan line and the limits of integration are from r_4 to r_5 along the (i,j) fan line of Fig. 2(b). This method has been previously used to design bolus for heavy charged particle beams: pions,[13] protons,[19,21] and heavy ions.[20] For heavy ions the particle range is sharply defined, as the multiple Coulomb scatter is significantly less than that for electrons.

For electrons this operator may still be useful for estimating bolus thickness in the presence of bone or fat. It is not particularly useful if large air cavities are present, conditions that are often encountered in the head and neck, particularly around the nasal opening and sinuses. Figure 3 illustrates the unusually shaped bolus and resulting dose distribution if bolus were so designed for anterior irradiation of the nose. As above, the operator **R** depends on two parameters, Δ and R_t, so $\mathbf{R} = \mathbf{R}(\Delta, R_t)$.

C. Modification operators

The idea of modifying the initial bolus design was first introduced for proton beams by Goitein[21] in an effort to make allowances for bolus misalignment. For proton dose distributions, because of the sharp distal and lateral dose gradients, effects due to scatter are small compared to misalignment errors (approximately 2–3 mm). In addition, treatment planners for proton therapy take advantage of the sharp beam delineation by reducing the physical target volume to match the biological target volume. As a result of scatter, the distal and lateral gradients of an electron dose distribution are smoother, so treatments are not generally planned with margin for setup errors. For example, one measure of scatter is the distance between the 80% isodose and the 20% isodose in the penumbra. For a 200-MeV proton beam, this distance is approximately 0.5 cm at 17-cm depth, while for a 15-MeV electron beam, this distance is approximately 1.5 cm at R_{90}. Electron multiple scattering has been shown to lead to dose inhomogeneities in the patient if it is not accounted for in the design of the bolus surface.[24] In the present work, patient movement and misalignment are ignored except within the clinical definition of a target volume.[27]

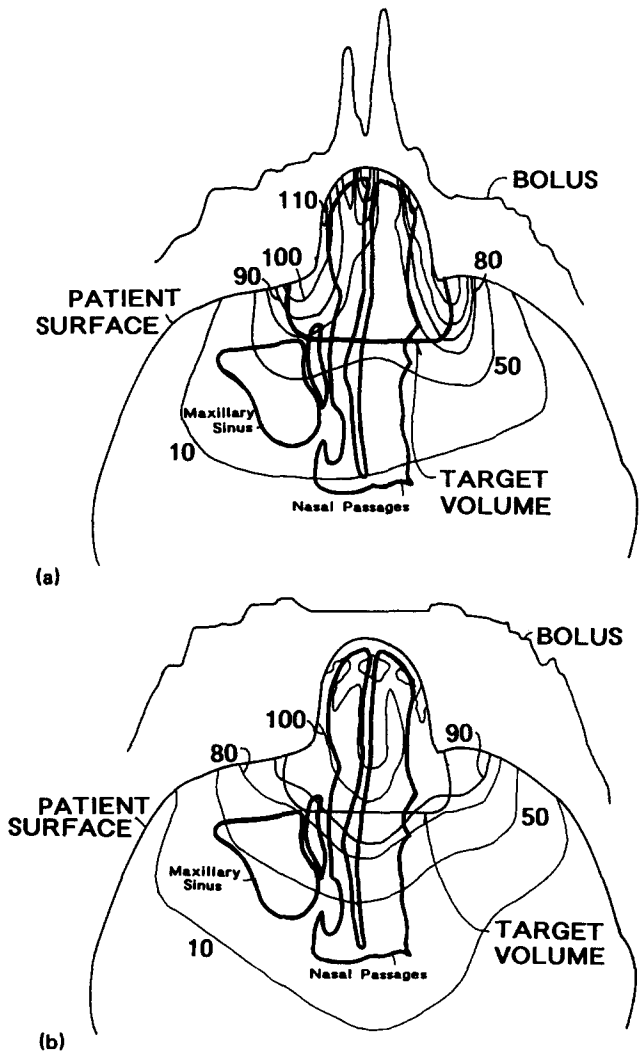

FIG. 3. A transverse slice through the nasal cavities with structure outlines determined from CT data showing the superimposed bolus and resulting dose distribution for a 17-MeV electron beam. (a) Bolus designed using the operator sequence $\mathbf{H}_t\mathbf{R}(0.1\text{ cm}, 6.0\text{ cm})$. Because of electron multiple scatter, the dose distribution is markedly heterogeneous, with the 90% isodose lines missing the target volume almost completely. (b) Bolus designed using the operator sequence $\mathbf{H}_t\mathbf{P}(0.1\text{ cm}, 6.3\text{ cm})$. The surface features generated by the **R** operator are absent, providing a more homogeneous dose distribution.

The first of the modification operators **I** is the isodose shift operator. This operator attempts to match the distal surface of the target volume with a planner-specified isodose contour, e.g., the isodose contour corresponding to a dose of 90% of the given dose. To execute this operator, the patient dose distribution is first calculated. For each fan line, the location of the point where it intersects the specified isodose surface is determined. The difference in effective depths between that point and the distal surface of the target volume is then added to (or subtracted from) the existing bolus. If the target isodose surface does not intersect the fan line, the bolus along that fan line is left unchanged. A similar manual technique based on differences in physical depth has been reported by Smith *et al.*[11] The isodose shift operator has only one parameter R_t so $\mathbf{I} = \mathbf{I}(R_t)$. This operator is considered a "one-dimensional" operator in that the bolus thickness along each fan line is modified using only information along that fan line.

The remaining modification operators are "three-dimensional," in that the bolus thickness along each fan line is modified using information from it and neighboring fan lines in both the x and y directions. Neighboring fan lines are defined to be within a radius of $\eta\sqrt{a_2}$, where for the fan line of interest, $\sqrt{a_2}$ is the root-mean-square value of a radial electron pencil-beam dose profile at the location where the fan line intersects the distal surface of the target volume. In a slab phantom (no x,y variation), values of η of 0.5, 1.0, and 2.0 encompass approximately 12%, 40%, and 86%, respectively, of the electrons reaching the distal surface of the target volume in the vicinity of the fan line of interest.

The modification operator $\mathbf{S}_t(\eta,\mu)$ smooths the bolus thickness by performing a weighted average of the neighboring bolus thicknesses. The bolus thickness for the (i,j) fan line is modified by

$$b_{ij} = \frac{\Sigma_{kl \ni \rho_{ijkl} < \eta\sqrt{(a_2)_{ij}}} b_{kl} \exp[-\mu\rho_{ijkl}^2/2(a_2)_{ij}]}{\Sigma_{kl \ni \rho_{ijkl} < \eta\sqrt{(a_2)_{ij}}} \exp[-\mu\rho_{ijkl}^2/2(a_2)_{ij}]}, \quad (4)$$

where $\rho_{ijkl} = |\boldsymbol{\rho}_{ij} - \boldsymbol{\rho}_{kl}|$ is the distance between the points where the (i,j) and (k,l) fan lines intersect the plane of isocenter, $(a_2)_{ij}$ is the value of a_2 for point 5 of Fig. 2(b), μ is

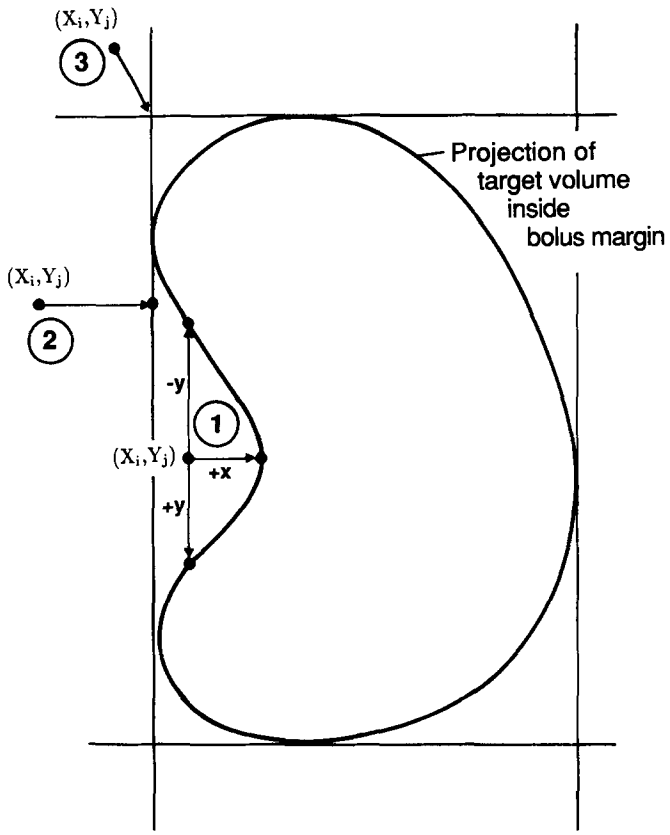

FIG. 4. Illustration of the actions of the bolus extension operators $\mathbf{H}_t$ and $\mathbf{H}_h$. The contour represents the projection onto a plane perpendicular to the central axis at isocenter of the target volume within the area of bolus design [cf. the dashed curve of Fig. 2(a)].

a weighting coefficient, and η governs the lateral distance over which the weighted average takes place. Strictly speaking, the value of a_2 should be taken relative to the (k,l) fan line at the same z position as that for point 5 of Fig. 2(b), and ρ_{ijkl} should also be determined at this z position. The approximations are employed for coding simplicity and to minimize calculation time. Large values of μ will oversmooth the bolus, yielding a homogeneous dose distribution at the expense of tracking the distal surface of the target volume, whereas small values of μ will be ineffective in smoothing the dose distribution. A similar operator $\mathbf{S}_h(\eta,\mu)$ smooths the height of the proximal surface of the bolus h_{ij} which in Fig. 2(b) is the z distance between points 2 and 3.

Operators have been designed for maximum coverage of the target volume $\mathbf{T}(\eta)$ and for maximum protection of a critical organ structure $\mathbf{C}(\eta,D_c)$. For the operator $\mathbf{T}(\eta)$, the bolus thickness along each fan line for which bolus thickness has been defined is set equal to the minimum value of itself and the bolus thicknesses along fan lines that both intersect the TVLM and are within the defined neighborhood:

$$b_{ij} = \min\left(b_{ij},\{b_{kl}\}^{kl\subseteq \mathrm{TVLM}}_{\rho_{ijkl}<\eta\sqrt{(a_2)_{kl}}}\right). \tag{5}$$

This operator is normally applied immediately after the creation operator $\mathbf{P}_t$ or $\mathbf{R}_t$ is used for the initial design. For example, the sequence of operators $\mathbf{TR}_t$ ($\mathbf{R}_t$ applied first) is similar to the design sequence used for protons by Goitein[21] and Urie *et al.*[19]

For the operator $\mathbf{C}$, the bolus thickness along fan lines intersecting the critical structure is modified such that the effective depth from the proximal bolus surface to the proximal critical structure surface equals the central axis depth at the dose value D_c in water. Then the bolus thickness along each fan line for which bolus thickness has been defined is set equal to the maximum value of itself and the bolus thicknesses along fan lines which both intersect the critical structure and are within the defined neighborhood:

$$b_{ij} = \max\left(b_{ij},\{b_{kl}\}^{kl\subseteq \text{critical structure}}_{\rho_{ijkl}<\eta\sqrt{(a_2)_{kl}}}\right). \tag{6}$$

This operator depends on D_c and η, i.e., $\mathbf{C} = \mathbf{C}(\eta,D_c)$.

D. Bolus extension operators

The bolus creation operators are capable of designing bolus only along fan lines that intersect the target volume, excluding any applied bolus margin. An extension operator is necessary to define the bolus beyond these limits in a manner that provides a usable dose distribution along the edges of the field.

An operator can be used to extend the bolus relative to either the bolus thickness ($\mathbf{H}_t$) or the proximal surface position, i.e., height ($\mathbf{H}_h$). This operator extends the bolus in three steps as shown in Fig. 4. Consider the operator $\mathbf{H}_h$: First, a rectangle (with edges parallel to the x and y axes) circumscribing the outer bolus margin is defined. The bolus surface heights are then determined for those areas within this rectangle where the bolus was previously undefined (shown as region 1). Each value of h is determined by calculating the harmonic mean of the surface heights of the nearest defined points along the x and y axes, referred to as h_{kl}, and is given by

$$h_{ij} = \sum_{m=1}^{4} \frac{(h_{kl})_m}{\rho_{ijkl}}\delta_m \left(\sum_{m=1}^{4}\frac{1}{\rho_{ijkl}}\delta_m\right)^{-1}. \tag{7}$$

In this equation, the sum over m is over the nearest intersections of lines drawn along the x and y axes with the boundary of the TVLM. The δ_m are equal to 1 if an intersection exists, and 0 if there is no intersection. For example, in Fig. 4, δ_m will be 1 for the line in the positive x direction, 1 for the lines in both the positive and negative y directions, and 0 for the line in the negative x direction, corresponding to the presence or absence of intersections of these lines with the boundary of the TVLM. The harmonic mean generates a smooth extension of the bolus while providing precise matching near previously defined points. The bolus is then extended parallel to the x and y axes within region 2, setting the surface positions equal to the positions of the nearest bolus point on the rectangle. Finally, bolus is extended to complete the remaining four corners of region 3. The bolus extension operator $\mathbf{H}_t$ is determined in the same manner with the heights (h) being replaced by bolus thicknesses (b).

The bolus operators are summarized by category in Table I. These operators have been incorporated for electrons into a 3-D treatment planning system[10] and are used for calculations of the results below.

Electron bolus is described mathematically in the 3-D treatment planning system. For a given treatment plan, each electron beam is assigned an individually designed bolus. For the calculation of dose, the mathematical description of

TABLE I. Summary of bolus design operators.

Operator	Description	Parameters	Type
P	Physical depth	Δ, R_t	Creation
R	Effective depth	Δ, R_t	Creation
I	Isodose shift	R_t	Modification
$\mathbf{S}_t$	Gaussian thickness smoothing	η, μ	Modification
$\mathbf{S}_h$	Gaussian height smoothing	η, μ	Modification
T	Maximum coverage	η	Modification
C	Critical structure avoidance	η, D_c	Modification
$\mathbf{H}_t$	Thickness extension		Extension
$\mathbf{H}_h$	Height extension		Extension

the bolus is incorporated into the effective depth and a_2 calculations.

III. RESULTS AND DISCUSSION

The beneficial effects of the use of bolus, as well as some of the limitations, can be shown through a series of examples that will each illuminate one or two particular difficulties inherent in the design of bolus. These include the effects of bolus surface irregularities, the slope of the distal surface of the target volume, and the sparing of critical structures. The bolus operators will be employed to account for these features, providing useful dose distributions. In all cases the 90% isodose is considered the minimum acceptable dose within the target volume. The distributions are normalized such that 100% represents the dose at $d_{\max}$ for a water phantom at the standard SSD (100 cm) for the rectangular field that circumscribes the irregular field.

While the dose is calculated using a 3-D heterogeneity correction, in order to facilitate evaluation of the operator functions, the phantom cross section is kept constant along the direction (y axis) perpendicular to the displayed plane for all cases except the nose and parotid, for which the three-dimensional patient anatomy was used.

A. Wedge target volume

The first phantom under consideration is a water phantom with a wedged-shaped target volume (see Fig. 5). Bolus must be used in this case to cause the prescription isodose to track the target volume and spare distal normal tissue.

Figure 5(a) shows the target volume and the bolus designed using the **P** creation operator (although the same result would have been obtained using the **R** creation operator, as the phantom is entirely water) in the operator sequence $\mathbf{H}_t\mathbf{P}$ (0.0 cm, 3.8 cm). The therapeutic depth R_t was selected to be 3.8 cm, with irradiation by a 15-MeV beam. This value, less than the R_{90} value in water of 4.5 cm, was selected because the therapeutic range shifts toward the surface if the surface is oblique with respect to the incident beam.[28] The proximal bolus surface exhibits sharply sloping and converging walls because of the shape of the distal surface of the target volume. Electrons that pass through the thicker portion of the bolus undergo more lateral scattering than those passing through the thin portion. The dose under the thin section of the bolus is therefore greater than that under the thick section, yielding a high-dose region. This hot spot serves to deepen the 90% isodose line near the center of the target volume. Similarly, the 90% isodose line becomes more shallow near the edges of the target volume.

The isodose shift operator with 90% as the target isodose is applied to the bolus of Fig. 5(a) to yield the bolus shown in Fig. 5(b). The operator sequence is

$\mathbf{H}_t\mathbf{I}(90\%)\mathbf{P}(0.0\text{ cm}, 3.8\text{ cm})$.

The resulting bolus surface exhibits some steep slopes and sharp discontinuities. However, the 90% isodose has moved closer to the distal surface of the target volume. The isodose shift operator can be applied an arbitrary number of times. Figure 5(c) shows the system after four applications of the operator. While the coincidence of the 90% isodose line and the target volume has improved, the bolus surface is quite contorted, leading to large dose inhomogeneities within the phantom. These contortions are caused by the one-dimensional nature of this operator. The asymmetry evident in the bolus shape is due to a combination of the iterative nature of the operator and a slight asymmetry of the accelerator output.

This case reinforces one of the difficulties with bolus design, namely that the requirement of congruence between a target volume surface and an isodose surface is insufficient to define the bolus. We conclude that one or two applications of the isodose shift operator may improve the congruence of the target isodose level and the distal surface of the target volume without introducing a significant level of dose inhomogeneity.

The most significant limitation of the isodose shift operator is the necessity of calculating the entire 3-D dose distribution. The computing time required for the calculation may render use of this operator unrealistic for a clinical setting with current computing methods. However, as computers continue to gain speed, use of this operator will become more feasible.

An application of the Gaussian smoothing algorithm is intended to decrease the effects of small-scale, deep-surface features. The Gaussian smoothing algorithm is applied to the bolus of Fig. 5(a) and the result shown in Fig. 6(a). The operator sequence was

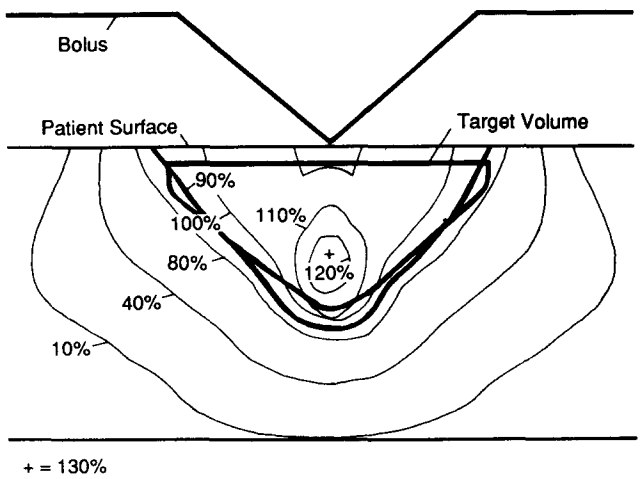

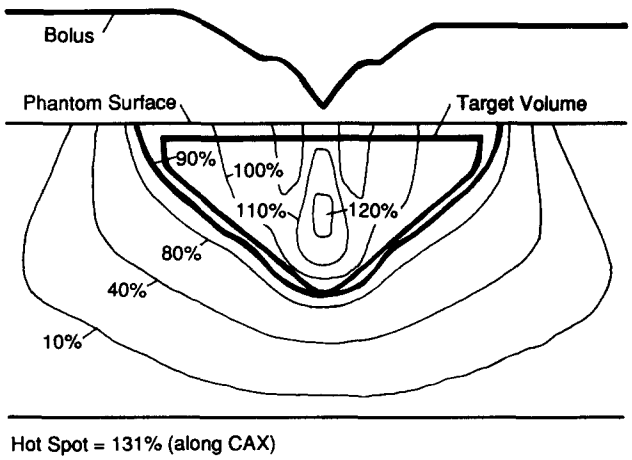

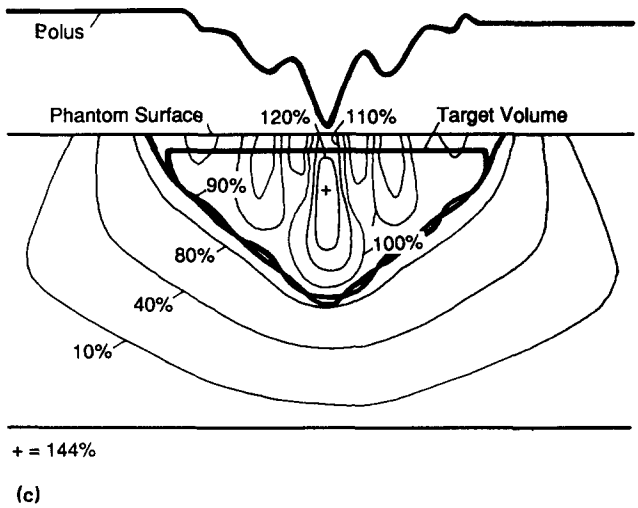

FIG. 5. (a) Wedge-shaped target volume in a water phantom irradiated by 15-MeV electrons with a bolus designed using the operator sequence $\mathbf{H}_t\mathbf{P}$ (0.0 cm,3.8 cm). (b) The isodose shift operator $\mathbf{I}$ is applied to the bolus in Fig. 1(a) through the operator sequence $\mathbf{H}_t\mathbf{I}(90\%)\mathbf{P}$(0.0 cm,3.8 cm). The congruence of the 90% isodose line with the target volume distal surface is improved at the cost of dose homogeneity within the target volume. (c) The isodose shift operator is applied four times to the target volume in Fig. 1(a). The congruence of the 90% isodose line with the target volume distal surface is nearly complete. However, the irregularly shaped bolus surface yields significant dose heterogeneities within the phantom.

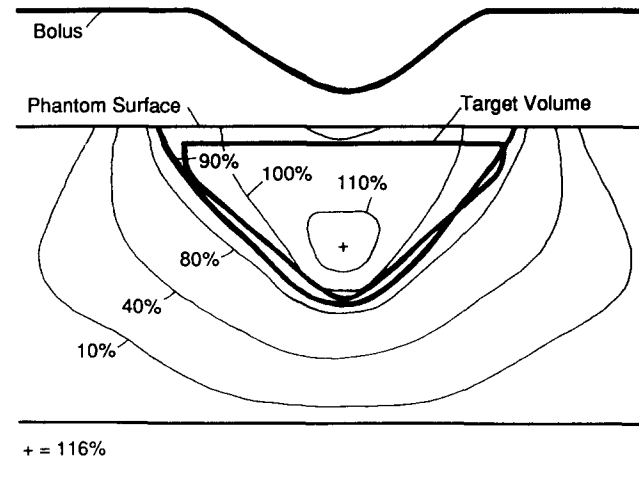

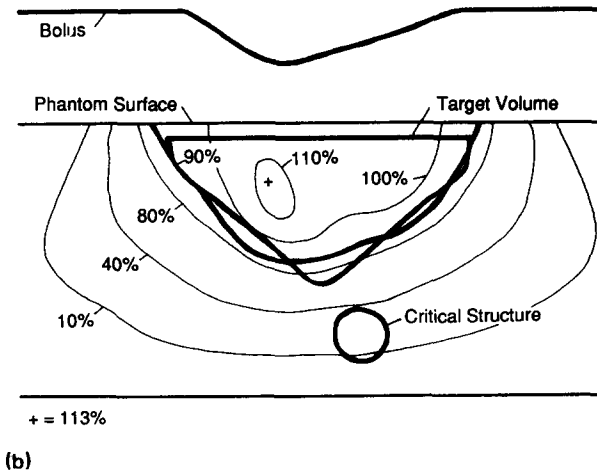

FIG. 6. (a) The bolus of Fig. 5(a) is modified using the Gaussian smoothing operator $\mathbf{S}$. The bolus design operator sequence is $\mathbf{H}_t\mathbf{S}_t(100,2.0)\mathbf{P}$(0.0 cm,3.8 cm). The severity of the hot spot is reduced, while the congruence of the 90% isodose line with the target volume is improved. (b) A critical structure has been added to the phantom. The critical structure avoidance algorithm is employed to add bolus material to limit the dose to the critical structure to less than 40%. The bolus design operator sequence is $\mathbf{H}_t\mathbf{S}_t\mathbf{C}$ (0.8,40%)$\mathbf{P}$(0.0 cm,3.8 cm). The added bolus material creates a cold spot near the distal margin of the target volume.

$$\mathbf{H}_t\mathbf{S}_t(100,2.0)\mathbf{P}(0.0\text{ cm},3.8\text{ cm}).$$

The value of $\eta = 100$ is equivalent to $\eta = \infty$, which was chosen to prevent the cutoff of the smoothing operator. The hot spot was reduced in size and severity (from 130% to 116%), while the agreement between the 90% isodose line and the target volume was improved. In general, values for η greater than 0.5 and μ between 0.2 and 2.0 are most useful. Values of μ smaller than 0.1 have little effect on the bolus surface, while a value of greater than 2.0 will excessively smooth the surface.

Figure 6(b) shows the same target volume as those in Figs. 5 and 6(a), with the addition of a critical structure. The critical structure avoidance operator is used to add bo-

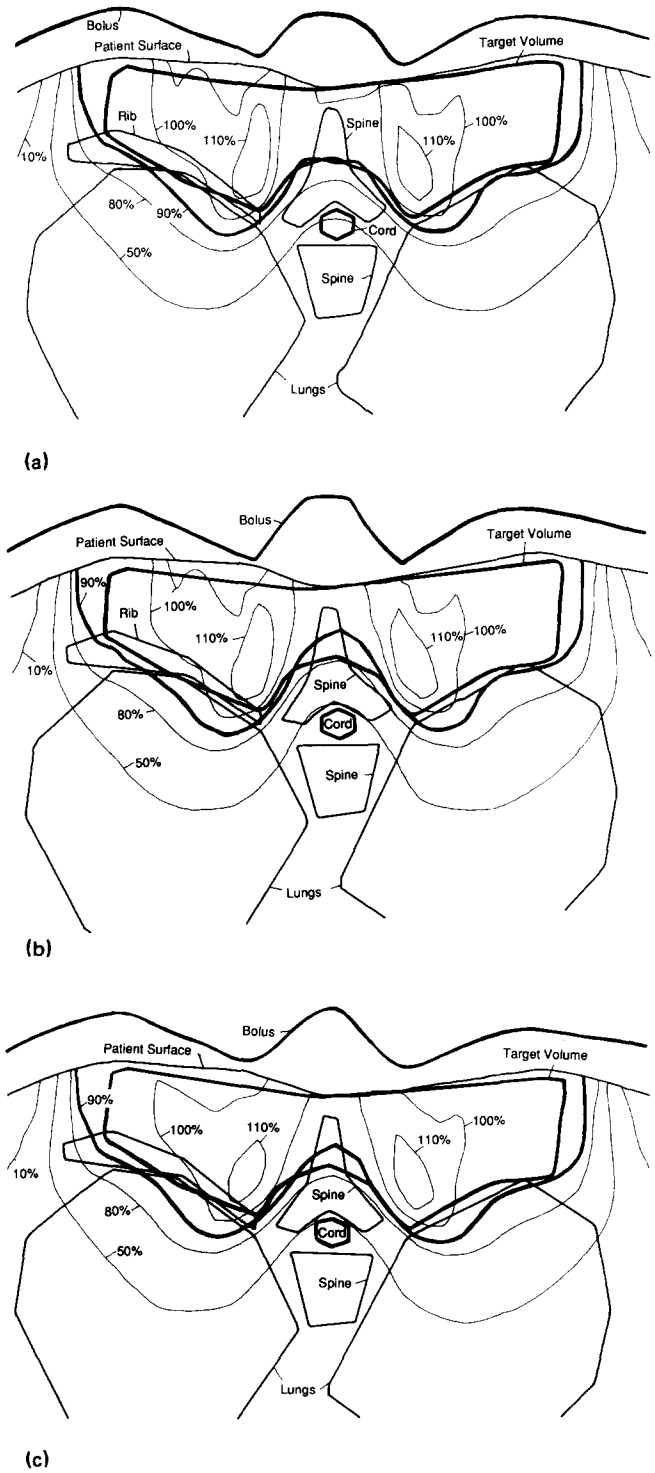

FIG. 7. (a) Paraspinal muscle irradiation using a 17-MeV electron beam and bolus designed with the **R** creation algorithm through the operator sequence $\mathbf{H}_t\mathbf{R}$(0.5 cm,4.9 cm). (b) The bolus shown in (a) is modified using the critical structure avoidance algorithm **C**. The operator sequence is $\mathbf{H}_t\mathbf{C}$(0.3,50%)**R**(0.5 cm,4.9 cm). (c) The smoothing algorithm $\mathbf{S}_t$ is applied to the bolus in (b), in the sequence $\mathbf{H}_t\mathbf{S}_t$(100,0.3)**C**(0.3,50%)**R**(0.5 cm,4.9 cm).

lus over the critical structure to bring the dose within the critical structure to less than 40%. The operator sequence is

$$\mathbf{H}_t\mathbf{S}_t(100,2.0)\mathbf{C}(0.8,40\%)\mathbf{P}(0.0\text{ cm},3.8\text{ cm}).$$

The added bolus material degrades the coincidence between the 90% isodose surface and the target volume. As expected, due to multiple scatter, the simultaneous requirements of critical structure sparing and target volume coverage cannot always be met.

B. Nose target volume

Patients frequently exhibit large density heterogeneities. The bolus, when designed using the creation algorithm and the radiological effective depth, may compensate for these internal heterogeneities. There are limitations of the effectiveness of this compensation. Figure 3(a) shows an outline of a transverse computed tomographic (CT) slice taken through the nasal vestibules. The patient dose calculation was performed for a 20-MeV electron beam. While this is the only slice shown, the bolus design and dose calculation was carried out in all three dimensions. The distal surface of the target volume is flat and featureless. However, there are distinct heterogeneities within and proximal to the target volume, primarily the nasal passages. When the effective depth creation algorithm **R** is used, through the operator sequence $\mathbf{H}_t\mathbf{R}$(0.1 cm,6.0 cm), the resulting bolus [shown in Fig. 3(a)] contains surface features that cause large dose inhomogeneities within the patient. For example, the hot spot dose is 122%. Figure 3(b) shows the same patient and CT slice, with a bolus designed using the physical depth creation algorithm **P** within the operator sequence $\mathbf{H}_t\mathbf{P}$(0.1 cm,6.3 cm). The hot spot has been reduced to 102%, with a corresponding reduction in the overall dose heterogeneity. However, the congruence between the 90% isodose surface and the target volume is still not ideal, with cold spots in the lateral margins. The congruence between the target volume margin and the 90% isodose line could be improved through the use of the isodose shift operator.

C. Paraspinal muscle irradiation

This bolus design example deals with the irradiation of the paraspinal muscles (shown in Fig. 7). This case offers some significant challenges for bolus design. The distal surface of the target volume contains some depressions and the spinal cord lies just beyond the target volume. Figure 7(a) shows the bolus designed by the effective depth creation operator in the sequence $\mathbf{H}_t\mathbf{R}$(0.5 cm,4.9 cm). The patient is irradiated with a 17-MeV electron beam. The bolus shape follows that of the target volume, causing an elevated region near the center. While this allows the 90% isodose surface to trace the target volume, it also causes two hot spots. The hot spots in turn deepen the 90% isodose near the portions of the target volume lateral to the spine.

The cord in Fig. 7(a) receives as much as 60% of the prescribed dose. Figure 7(b) shows the effect of applying the bolus addition operator and setting the desired maximum dose to 50%. The operator sequence was $\mathbf{H}_t\mathbf{C}$(0.3,50%)**R**(0.5 cm,4.9 cm). The maximum cord dose has decreased to slightly less than 50%, but the high-dose regions have become slightly larger. The 90% isodose surface also enters the target volume proximal to the spinal cord because of the increased bolus thickness.

The hot spots can be reduced somewhat by the application

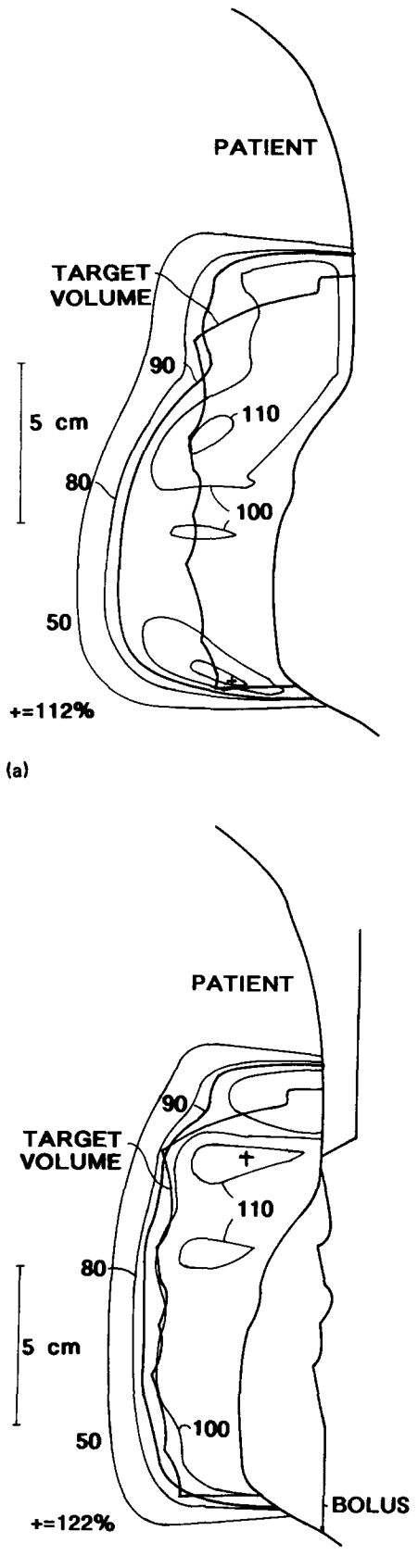

FIG. 8. Coronal view including the central axis of a parotid irradiation using 17-MeV electrons. (a) The dose distribution with no bolus. (b) The dose distribution using bolus designed by the operator sequence $\mathbf{H}_t\mathbf{P}(1.5\text{ cm},5.4\text{ cm})$. The value of $\Delta = 1.5$ cm was chosen to avoid most of the steep slope of the edge of the target volume in the cephalic direction.

of the Gaussian smoothing algorithm. Figure 7(c) shows the bolus generated with the sequence

$$\mathbf{H}_t\mathbf{S}_t(100,0.3)\mathbf{C}(0.3,50\%)\mathbf{R}(0.5\text{ cm},4.9\text{ cm}).$$

The smoothed bolus provides smaller high-dose regions while maintaining adequate cord sparing.

D. Parotid irradiation

Target volumes in three dimensions present one of the common difficulties in radiotherapy. An electron energy suitable for irradiation of one transverse slice may be unsuitable in a neighboring plane. This is the case illustrated in Fig. 8 which shows a coronal view along the central axis of a parotid irradiation where the depth of the target volume has a substantial gradient. The bolus was generated using the operator sequence $\mathbf{H}_h\mathbf{P}(1.5\text{ cm},5.4\text{ cm})$ and the patient irradiated with a 17-MeV electron beam. Figure 8(a) shows the dose distribution without bolus. The high energy is required to penetrate to the distal extension of the cephalic region of the target volume. This causes a significant irradiation of uninvolved tissue distal to the caudal region of the target volume. Figure 8(b) shows the patient irradiated with the same beam geometry and energy as in Fig. 8(a), but with bolus. Several differences between the two dose distributions should be noted. First, the bolus causes the therapeutic 90% isodose to match the distal surface of the target volume more closely throughout the coronal slice. Thus the primary goal of bolus design has been achieved. Second, the area enclosed by the 100% isodose has increased significantly due to the presence of the overlying bolus effectively shifting the SSD toward the source. Third, dose heterogeneities have increased due to irregularities in the bolus surface caused by the shape of the distal surface of the target volume. The irregular shape of the distal surface of the target volume was the result of outlining target volumes in individual transverse planes without smoothing over adjacent transverse planes. Gaussian smoothing of the bolus surface should improve the homogeneity of the target volume dose with little effect on the dose-target volume conformation. Finally, a significant amount of healthy tissue is still being treated adjacent to the superior boundary of the target volume. This is because the 1.5-cm bolus margin terminated the bolus design at a point where the distal surface of the target volume is still rather deep. A decreased bolus margin would place additional bolus over the superior margin of the target volume and reduce the dose to uninvolved tissue in that region.

IV. SUMMARY

It has been demonstrated that there is usually no solution to the general problem of designing a bolus that results in a uniform dose distribution conformed to the target volume. A methodology that allows alteration of the dose distribution using bolus operators is presented. These operators create, modify, and extend the bolus shape. Examples demonstrate how, through the proper use of operator sequences, improvements to the dose distribution can be made. No attempt was made in the present work to demonstrate usage of the operators to obtain an optimized dose distribution. Most of the operators are quickly executed in the treatment plan-

ning system in that they do not require the calculation of dose.

In some cases (e.g., the paraspinal muscles) the creation operator based on effective depths is applied and provides a more useful bolus than one based on physical depths. However, in other cases (e.g., the nose), the creation operator based on physical depth is preferable to one based on effective depth. In general, the dose uniformity in the target volume can be improved by the use of modification operators that smooth the bolus. Modification operators that interrogate surrounding bolus thickness can both improve coverage of the target volume and minimize dose to a critical structure.

Special design of bolus near the edge of the projection of the target volume is done by limiting creation operators to a margin Δ inside the target volume and then extending the bolus to well outside the treatment field using a technique based on the harmonic mean. The limitation and extension are necessary to reduce dose inhomogeneity near the edge of the target volume.

Although bolus can be designed using operators, to fully appreciate the utility of bolus, it is necessary to calculate the dose distribution in 3D with the bolus present. It is also useful to display the bolus shape on the patient CT to assist in understanding the resulting dose distribution. This can be particularly useful if additional bolus operators are to be applied.

We believe this methodology to be a reasonable approach to the design of bolus in a clinical setting. As more experience is gained with the system, it may be possible to design a knowledge-based system that could automatically select the bolus operator sequence for a particular treatment site.

ACKNOWLEDGMENTS

This work has been supported in part by NCI Grant CA-06294 and NCI contract CM-67914.

[a] Present address: Mallinckrodt Institute of Radiology, Division of Radiation Oncology, 510 South Kingshighway, St. Louis, MO 63110.

[1] K. R. Hogstrom, "Dosimetry of electron heterogeneities," in *Advances in Radiation Therapy Treatment Planning*, AAPM Monograph #9, edited by A. Wright and A. Boyer (American Institute of Physics, New York, 1983), pp. 223–243.

[2] K. R. Hogstrom and R. S. Fields, "The use of CT in electron beam treatment planning, current and future development," in *Computerized Tomography in Radiation Therapy*, edited by C. Ling, C. Rogers, and R. Morton (Raven, New York, 1983), pp. 223–243.

[3] R. F. Moyer, W. R. McElroy, J. C. O'Brien, and C. C. Chamberlain, "A surface bolus material for high-energy photon and electron therapy," Radiology **146**, 531–532 (1983).

[4] R. F. Moyer, G. A. King, and J. F. Hauser, "Lead as surface bolus for high-energy photon and electron therapy," Med. Phys. **13**, 263 (1986).

[5] D. M. Galbraith and J. A. Rawlinson, "Partial bolussing to improve the depth doses in the surface region of low energy electron beams," Int. J. Rad. Onc. Biol. Phys. **10**, 313–317 (1984).

[6] R. E. Haselow, F. M. Kahn, S. C. Sharma, and J. Williamson, "Water bag bolus in external air cavities to produce dose homogeneity," Int. J. Rad. Onc. Biol. Phys. **8**, 137–139 (1982).

[7] J. O. Archambeau, B. Forell, R. Doria, D. O. Findley, R. Jurisch, and R. Jackson, "Use of variable thickness bolus to control electron beam penetration in chest wall irradiation," Int. J. Onc. Biol. Phys. **7**, 835–842 (1981).

[8] J. L. Beach, C. W. Coffey, and J. S. Wade, "Individualized chest wall compensating bolus for electron irradiation following mastectomy: An ultrasound approach," Int. J. Onc. Biol. Phys. **7**, 1607–1611 (1981).

[9] D. R. Ruegsegger, S. D. Lerude, and D. Lyle, "Electron-arc therapy using a high energy betatron," Radiology **133**, 483–489 (1989).

[10] G. Starkschall, S. W. Bujnowski, L. L. Wang, D. A. Low, and K. R. Hogstrom, "Effect of dimensionality of heterogeneity corrections on the implementation of a three-dimensional electron pencil-beam algorithm," Phys. Med. Biol. **36**, 207–227 (1991).

[11] R. M. Smith, J. M. Galvin, M. Needham, A. R. Smith, and R. L. Goodman, "Computer-aided design and fabrication of electron and photon compensators," to be published in Int. J. Rad. Onc. Biol. Phys.

[12] K. R. Hogstrom, A. R. Smith, J. W. Somers, R. G. Lane, I. I. Rosen, S. L. Simon, and C. A. Kelsey, "Measurement of the effect of inhomogeneities and compensating bolus in clinical pion beams," Med. Phys. **6**, 26–31 (1979).

[13] K. R. Hogstrom, A. R. Smith, S. L. Simon, J. W. Somers, R. G. Lane, I. I. Rosen, C. A. Kelsey, C. F. von Essen, M. M. Kligerman, P. A. Berardo, and S. M. Zink, "Static pion beam treatment planning of deep seated tumors using computerized tomographic scans," Int. J. Onc. Biol. Phys. **5**, 875–886 (1979).

[14] H. A. Wright, J. E. Turner, and R. N. Hamm, "Effects of a bolus and inhomogeneities on pion stopping distributions," Med. Phys. **11**, 751–754 (1984).

[15] M. S. Wagner, "Automated range compensation for proton therapy," Med. Phys. **9**, 749–752 (1982).

[16] C. L. Wingate, J. O. Archambeau, A. M. Koehler, and G. W. Bennett, "Proton penetration and control in nonhomogeneous phantoms," Med. Phys. **4**, 198–201 (1977).

[17] M. M. Urie, J. M. Sisterson, A. M. Koehler, M. Goitein, and J. Zoesman, "Proton beam penumbra: effects of separation between patient and beam modifying devices," Med. Phys. **13**, 734–741 (1986).

[18] A. Akanuma, R. Okamoto, Y. K. Nakamura, H. Tsunemoto, S. Morita, T. Arai, A. Kurisu, T. Hiraoka, K. Kawachi, and T. Kanai, "Compensation techniques in NIRS proton beam radiotherapy," Int. J. Rad. Onc. Biol. Phys. **8**, 1629–1635 (1982).

[19] M. Urie, M. Goitein, and M. Wagner, "Compensating for heterogeneities in proton radiation therapy," Phys. Med. Biol. **29**, 553–566 (1983).

[20] G. T. Y. Chen, R. P. Singh, J. R. Castro, J. T. Lyman, and J. M. Quivey, "Treatment planning for heavy ion radiotherapy," Int. J. Onc. Biol. Phys. **5**, 1809 (1979).

[21] M. Goitein, "Compensation for inhomogeneities in charged particle radiotherapy using computed tomography," Int. J. Radiat. Oncol. Biol. Phys. **4**, 499 (1978).

[22] J. W. Andrew and B. J. McParland, "An automated system for the production of bolus for electron beam treatments," in *The Use of Computers in Radiation Therapy*, edited by I. A. D. Bruinvis *et al.* (Elsevier, North Holland, 1987), pp. 315–318.

[23] M. Takizawa, S. Sone, T. Watanabe, Y. Imai, S. Imai, and M. Miyazawa, "An interactive desk-top compensating filter maker using compact 3-D NC-Mill," in *The Use of Computers in Radiation Therapy*, edited by I. A. D. Bruinvis *et al.* (Elsevier, North Holland, 1987), pp. 307–310.

[24] K. R. Hogstrom, "Treatment planning in electron-beam therapy," in *Frontiers in Radiation Therapy Oncology*, edited by J. M. Vaeth, J. L. Meyer (Karger, Farmington, CT, 1991), pp. 25, 30–52.

[25] K. R. Hogstrom, "Evaluation of electron pencil beam dose calculation" in *Radiation Oncology Physics*, AAPM Monograph #15, edited by J. G. Kereiakes, H. R. Elson, and C. G. Born (American Institute of Physics, New York, 1987), pp. 532–557.

[26] K. R. Hogstrom, M. D. Mills, and P. R. Almond, "Electron beam dose calculations," Phys. Med. Biol. **26**, 445–459 (1981).

[27] *Dose Specifications for Reporting External Beam Therapy with Photons and Electrons*, ICRU 29 (1978).

[28] K. E. Ekstrand and R. L. Dixon, "The problem of obliquely incident beams in electron-beam treatment planning," Med. Phys. **9**, 276–278 (1982).